processes

MDPI

Article

The Upper Triassic Braided River Thin-Bedded Tight Sandstone in the Yanchang Formation, Ordos Basin: Sedimentary Characteristics, Seismic Forecasting Method, and Implication

Tongyang Lou [1,2], Congjun Feng [1,2,*], Mengsi Sun [3] and Zhiqiang Chen [1,2]

[1] State Key Laboratory of Continental Dynamics, Northwest University, Xi'an 710069, China; loutyang123@163.com (T.L.)
[2] Department of Geology, Northwest University, Xi'an 710069, China
[3] School of Petroleum Engineering and Environmental Engineering, Yan'an University, Yan'an 716000, China
* Correspondence: fengcj@nwu.edu.cn

Abstract: In the Ordos Basin, Chang 81, a Member of the Yanchang Formation, features the development of braided river thin-bedded tight sandstones. These sandstones constitute one of the main production layers of tight oil and gas in the Yanchang Formation within the basin. This study integrates data from core samples, drilling, and seismic information to identify braided river thin-bedded sandstones in the Chang 81 Member at Daijiaping, Ordos Basin, using a method of constrained correlation between seismic waveform and seismic facies. This approach aids in determining the sedimentary microfacies types and reservoir characteristics of thin-bedded tight sandstones. We establish a quantitative fitting formula for the width-to-thickness ratio of braided channel sand bodies to finely characterize sand body stacking patterns and spatial distribution of thin-bedded tight sandstones in braided channels. Braided delta plain deposits in the Chang 81 Member at Daijiaping mainly comprise four types of sedimentary microfacies: braided channels, crevasse channels, floodplains, and swamps. The thickness of the reservoir sand body of Chang 81 member is mainly concentrated between 5–25 m, with low porosity and permeability, making it a typical thin-bedded tight sandstone reservoir. A method of constrained correlation between seismic waveforms and seismic facies was employed to identify sand bodies of braided river thin-bedded sandstones in the Chang 81 Member, summarizing four sand body stacking patterns: longitudinal incision type, longitudinal separation type, lateral shifting type, and single channel type. Furthermore, a quantitative forecasting formula of width-to-thickness ratio was established for the river channel scale, providing accurate guidance for well deployment. Horizontal wells deployed from the sand body's side towards its center in a river channel yield a production 1.8 times higher than that of horizontal wells deployed in the opposite direction. Thin-bedded tight sandstones in braided channels, characterized by flat-top and convex-bottom lenticular seismic facies, hold practical significance in guiding the deployment of horizontal well patterns for tight oil and enhancing oil and gas recovery.

Keywords: braided river; tight sandstone; seismic facies; sandbody architecture

Citation: Lou, T.; Feng, C.; Sun, M.; Chen, Z. The Upper Triassic Braided River Thin-Bedded Tight Sandstone in the Yanchang Formation, Ordos Basin: Sedimentary Characteristics, Seismic Forecasting Method, and Implication. *Processes* **2023**, *11*, 1303. https://doi.org/10.3390/pr11051303

Academic Editors: Yang Wang and Wenyang Shi

Received: 18 March 2023
Revised: 15 April 2023
Accepted: 20 April 2023
Published: 22 April 2023

1. Introduction

As the world's energy needs continue to grow, so do the challenges associated with exploration and development in new areas, especially as most of the easy-to-find oil and gas reserves have already been discovered [1–5]. As a result, oil exploration has gradually shifted to a more challenging environment. Thin tight sandstone has become the focus of oil and gas exploration in recent years and will become the most important source of oil and gas resources in the next 10 to 20 years. Therefore, how identifying and predicting thin, tight sandstone has become the top priority in the field of oil and gas in the future.

At present, seismic forecasting of thin-bedded tight sandstone is an active and challenging issue in the field of sedimentary basin oil and gas exploration and research. In

recent years, scholars worldwide have conducted extensive research on the geological characteristics, sedimentary genesis, and reservoir prediction of thin-bedded tight sandstone, achieving fruitful results [6–14]. The significant progress in this area can be summarized in three aspects:

(1) Tight sandstone reservoirs are characterized by deep burial depth, complex diagenetic evolution, poor reservoir physical properties [8,15,16], and strong heterogeneities that can influence fluid recovery in aquifers and reservoirs [17,18].

(2) The sedimentary genesis of tight sandstones is mainly reflected in a relatively slow deposition rate [19], weak and stable hydrodynamic conditions, distinct interbedding structures in the formation [20,21], and frequent association with delta deposits [22].

(3) Experts and scholars have used various techniques to predict tight sandstone reservoir properties, achieving good results. Castagna, Golshubin, and Beatriz [6,7,9] successfully identified thin-bedded sandstone reservoirs using low-frequency information below 6 Hz. Zhou [10] proposed a decomposed prediction MEM based on well-seismic data to address the quantitative prediction problem of thin-bedded sand bodies in meandering stream facies in the Dagang X development zone. He established the relationship between the thickness of thin-bedded sand bodies and the tuning thickness by fitting the drilling data, thereby completing the quantitative prediction of thin-bedded sand bodies. Chen [12] used pre-stack phase inversion, multiple inversion, and encrypted synchronous frame-constrained sliding threshold methods to characterize thin-bedded sand bodies and design a horizontal well trajectory under conditions of thin sand bodies in the Fuyu oil layer, unstable distribution, and large lateral variations, achieving a sandstone encounter frequency of 99.5% for horizontal wells.

Due to the attenuation of seismic wave energy caused by Quaternary deep-bedded loess layers in the Ordos Basin [23–25], a strong reflection of controlled lineup energy by thick shale at the bottom of the Chang 7 Member, and thin braided river tight sandstone in the Chang 81 Member, predicting thin-bedded sand bodies in the study area is challenging. Seismic attributes, freeze-drying microtomy of stratigraphic facies, and sparse impulse inversion constrained by well logging have all been attempted but with limited success.

For these reasons, (i) this study employs a method of constrained correlation between seismic waveform and seismic facies to identify braided river thin-bedded sandstones in the Chang 81 Member at Daijiaping, Ordos Basin; (ii) The sedimentary microfacies types and reservoir characteristics of thin tight sandstone were determined by the comprehensive application of core, drilling and logging data.; (iii) Combined with seismic, drilling, and logging data, sand body stacking patterns and the spatial distribution of thin-bedded tight sandstones in braided channels are finely characterized. Thin-bedded tight sandstones in braided channels, characterized by flat-top and convex-bottom lenticular seismic facies, have practical significance in guiding the deployment of horizontal well patterns for tight oil and improving oil and gas recovery.

2. Geologic Setting

Located in the western part of the North China Platform, the Ordos Basin is a craton basin formed by the stacking of the Paleozoic platform, marginal depression, and the Mesozoic-Cenozoic intra-platform depression [26–28]. With a wide and gentle eastern flank and a steep and narrow western flank, it is an asymmetric rectangular synclinal basin with a total area of 25×10^4 km^2 and is also the second-largest oil and gas-bearing basin in China. The Ordos Basin can be further divided into six SBUs: Yimeng uplift, Western edge thrusting belt, Tianhuan depression, Yishan slope, Jinxi flexural fold belt, and Weibei uplift (Figure 1a) [29,30]. Multiple oil-bearing series develop in the Ordos Basin. The Yanchang Formation of the Upper Triassic series is the main oil and gas-bearing horizon of the Mesozoic erathem in the Ordos Basin [31].

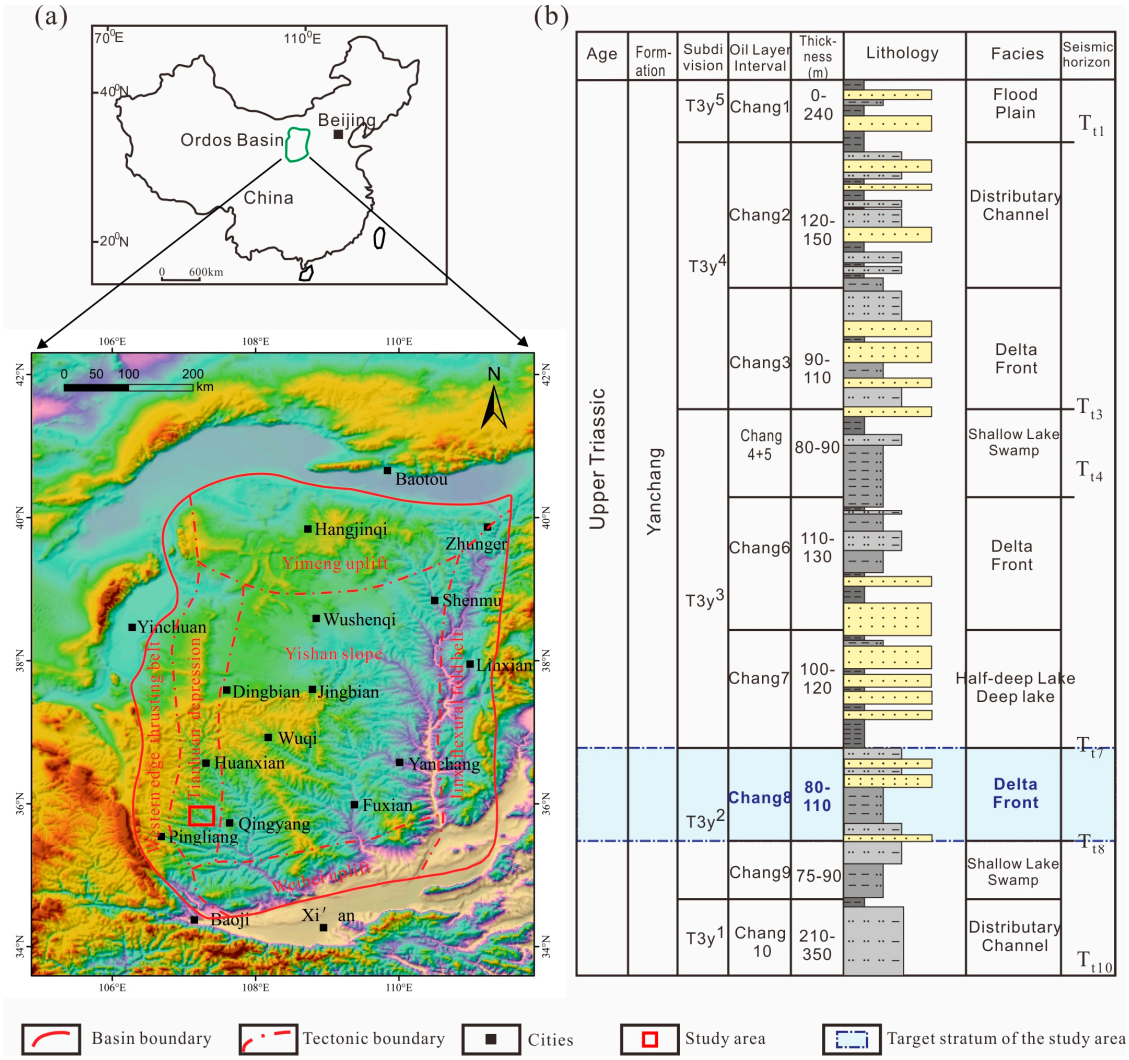

Figure 1. Geologic Setting Map of the Study Area (**a**) Geographical Location Map of the Study Area; (**b**) Stratigraphic Column of the Study Area.

The study area is located in Daijiaping, southwest of the Ordos Basin, north of the Weibei uplift, and south of the Tianhuan Depression. The structure of the study area is relatively gentle, showing the overall west-dipping monocline structure, lack of large structures, mainly small nose uplift, covering an area of about 2515.68 km^2. The study area has experienced several multi-stage tectonic movements, among which the Indosinian, Yanshanian, and Xishan tectonic movements have a great influence on the structural morphology of this area. The result is the contact relation of disconformity or parallel unconformity among some strata in the study area [32]. The Yanchang Formation of the Upper Triassic, which was formed in the late Triassic braided river delta, is the main oil-bearing horizon in this area. A suite of light gray fine sandstone, siltstone, and dark mudstone develops in the oil formation of the C8 member, the main oil-bearing horizon, which is a typical type of shallow delta front-edge deposit [33–36] (Figure 1b). It has characteristics such as fine sand body size, large thickness change, and rapid sedimentary facies changes. The C8 member of the Yanchang Formation in Daijiaping is about 80–110 m thick and is divided into two sub-layers from top to bottom: C81 and C82. C81 consists of C811, C812 and C813 layers. C82 consists of two layers, C821 and C822. Sandstone is mainly developed in C812, and a few sand bodies are developed in C813. The thickness of the sandstone is 5–25 m. A suite of gray-black C7 member Zhangjiatan shale is developed

on the top of the C8 member. In this paper, the C7 member shale is regarded as a marker bed to identify thin-bedded sandstone in the Chang 81 member.

3. Data and Method

This study was carried out using core data from approximately 100 m in 7 cored wells, data from 32 exploration and appraisal wells, data from 2 horizontal wells, and post-stack 3D seismic data. The 3D seismic data, covering an area of about 700 km^2, has a relatively high signal-to-noise ratio (SNR) and resolution, with a bandwidth of 15–45 Hz and a dominant frequency of 20–35 Hz. The elevation of the 3D seismic datum in the study area is 1400 m, the seismic profile is positive polarity, and the wavelet is 0 phase. The dominant frequency of the target stratum (Chang 81 member sand body) is about 35 Hz. Seismic data were sampled every 2 ms, with the surface element size being 25 m × 12.5 m. ① Based on core marks, petrophysical calibration of logging curves (natural gamma ray, acoustic log, and density curves), and sedimentary characteristics, typical sedimentary microfacies of the C81 member were comprehensively identified, and seven lithofacies types were summarized. ② Combining logging data, seismic facies, and characteristics of sedimentary microfacies, channel stacking patterns were analyzed using well-seismic data based on seismic profiles, and the stacking characteristics and distribution patterns of four types of braided channels were identified. ③ The thin sandstone of the C81 member in the study area was identified by the method of constrained correlation between seismic waveform and seismic facies, and the lenticular seismic facies of the C81 member was explained in detail. The lenticular seismic facies characteristics were revealed according to the drilling, and the transverse distribution range of the braided channel sandstone was described. ④ According to the statistical results for braided river lenticular seismic facies calibrated on 32 wells in the study area, including the bank's full width and the maximum depth, a quantitative forecasting formula of width-to-thickness ratio was established for the river channel scale. ⑤ Based on the calibrated lenticular seismic facies using well-seismic data, two different horizontal well drilling plans were compared to reveal the guiding significance of distribution characteristics of seismic facies combined with well-seismic data to guide the well pattern deployment of tight oil horizontal Wells.

The main idea of the method of constrained correlation between seismic waveform and seismic facies is to use the data body of seismic waveform, and fill the wave crest part with black-filled variable areas in the seismic waveform section, while the trough is not filled, so as to better identify the continuity of wave crest (or trough). Channel sand bodies in seismic facies are usually characterized by down-cut lenticular features of "flat-top and convex-bottom", and channel lens bodies are characterized by continuous wave crest in the phase axis (or white wave trough in phase axis) and obvious downward curvature in waveform section. Therefore, the method of constrained correlation between seismic waveform and seismic facies can make the identification of channel lens sandstone easier and more accurate. As a result, the shale bed at the bottom of the C7 member is corrected as a flat reference surface and used as a marker bed. According to the calibrated synthetic seismogram of wells that encounter sand bodies during drilling, sandstones observed after drilling on the Chang 81 Member exhibit "flat-top and convex-bottom" lenticular seismic facies on seismic profiles. In other words, continuous wave peak lineups (or white wave trough lineups) at black-filled variable areas on waveform profiles exhibit a distinct downward curvature. Moreover, the lateral extent of such lenticular seismic facies exactly represents the lateral extent of braided river sandstones. Then, the lateral extent of braided river sandstones observed after drilling can be presented using such lenticular seismic facies observed after drilling as well-seismic data for sandstone calibration. Based on calibrated lenticular seismic facies of known well points, the extent of lenticular seismic facies for areas where no drilling is carried out is determined every 10 seismic lines, and then the inter-well braided river sand bodies were identified.

4. Results

4.1. Types and Characteristics of Sedimentary Microfacies

Facies marker characteristics such as mudstone color, bedding structure, and fossil features were analyzed based on core observations and descriptions. In the geological context of the study area, Chang 81 Member of the Yanchang Formation in Daijiaping was mainly considered as the braided delta plain subfacies, covering four microfacies, including braided channels, crevasse channels, floodplains, and swamps.

4.1.1. Braided Channel Microfacies

Description

Braided channel microfacies include four typical facies assemblages (FAs): parallel-bedded sandstone facies (Sh), tabular cross-bedded sandstone facies (Sp), trough cross-bedded sandstone facies (St), and massive-bedded pebbly sandstone facies (Gpt) (Figure 2, Table 1). Parallel-bedded sandstone facies are mainly composed of gray fine- to medium-grained sandstone and argillaceous siltstone, about 1–3 m thick, and develop into parallel bedding (Figure 2c). Tabular cross-bedded sandstone facies develop in the middle part of braided channels, about 2–3 m thick. It mainly consists of gray fine- to medium-grained sandstone. Black laminations are often carbonaceous laminations (Figure 2a) in abrupt contact with the massive sandy conglomerate. Trough cross-bedded sandstone facies, about 2 m thick, are mainly composed of gray-white fine–coarse sandstone with no paleontological fossils. Massive-bedded pebbly sandstone facies, about 1 m thick, are distributed at the bottom of trough cross-bedded sandstone and tabular cross-bedded sandstone, with large lateral thickness changes. Conglomerate, 1–6 cm long and 0.5–2 cm thick, is mostly flat, irregularly distributed, and directionally arranged (Figure 2d). Braided channel sandstones have gamma values of 50–80 API. The gamma curve is characterized by dentate bell-shaped and dentate box-shaped patterns (Figure 2f).

Explanation

A large number of erosion surfaces, unidirectional flow of trough and tabular cross-bedded sandstones, and upward fine-grained cycles topped by parallel bedded fine sandstones indicate typical fluvial deposits. Conglomerate-bearing sandstones at the base of the sandstones indicate lag deposits on the river bed. Conglomerate, usually in irregular geometry, has a roundness of angular-subangular shape, showing that they were formed by the flow of water eroding the mudstone on both sides of the upstream river bed before proximal transportation and deposition, reflecting the characteristics of strong hydrodynamic force and erosion capability. The repeated occurrence of massive pebbled sandstone facies indicates that braided channels have multi-stage cycles and multi-period channel stacking [37–41].

4.1.2. Crevasse Channel Microfacies

Description

Crevasse channel microfacies are associated with tabular cross-bedded sandstone facies (Sp) (Figure 2, Table 1) and are characterized by fine gray sandstone with a thin single-bed thickness, typically 1–2 m thick. These channels exhibit small planar cross-bedding and erosion surface structures and are clearly undercut (Figure 2e). The top and bottom surfaces are surrounded by mudstone and make contact with the underlying mudstone through scouring action (Figure 2e). The gamma curve is finger-shaped or small bell-shaped, with gamma values of 50–150 API (Figure 2f).

Explanation

Crevasse channels are rare in the study area. The scouring surface at the bottom (Figure 2e) indicates that the hydrodynamic force of the river channel increases rapidly during the crevasse period, resulting in a higher flow velocity. In this case, the underlying swamp mudstone is scoured and eroded, forming an uneven scouring surface. The

abrupt change in the gamma curve to a finger-shaped pattern also reflects the alternating hydrodynamic conditions of the river channel during the crevasse period.

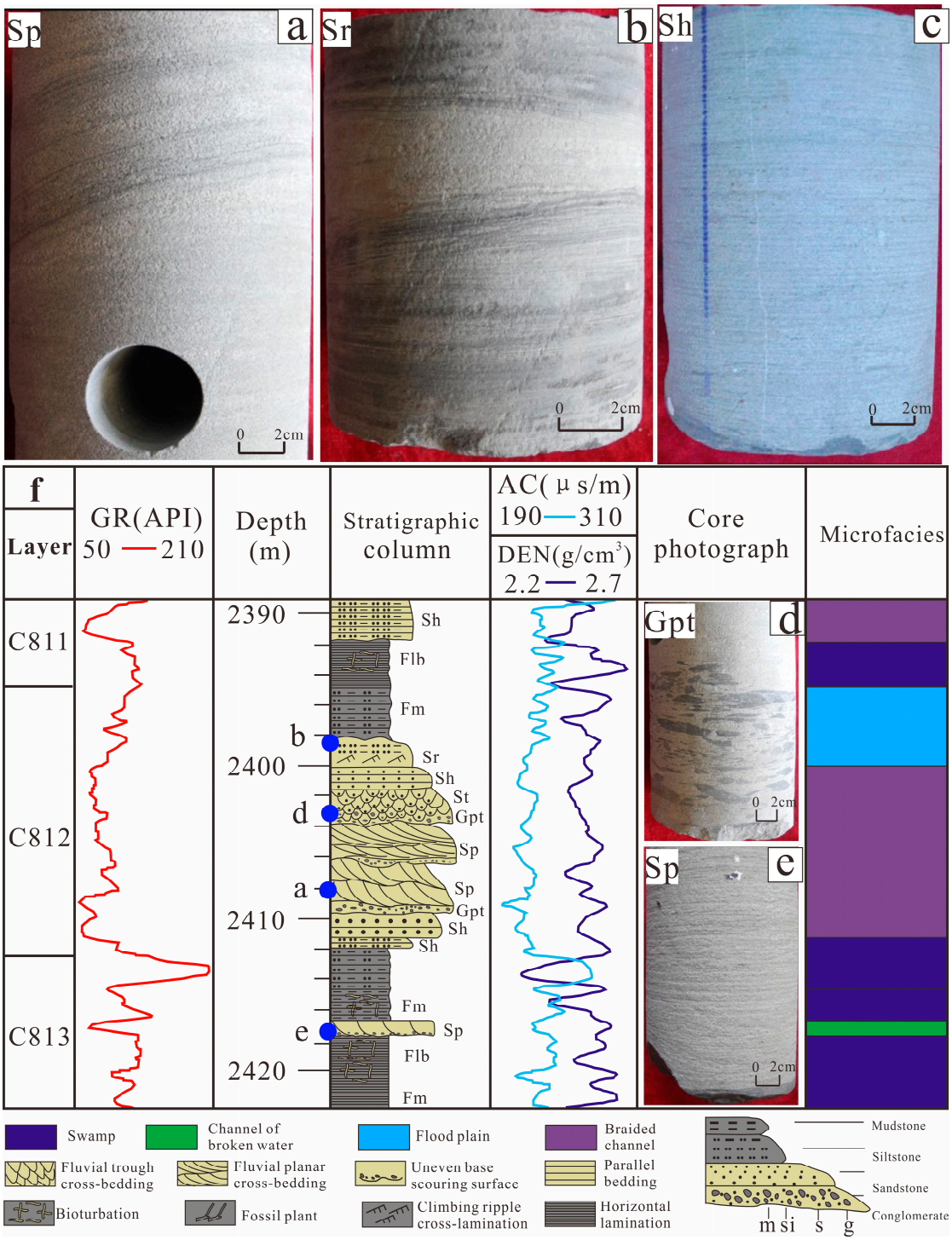

Figure 2. Photographs and stratigraphy of the Chang 8 member in Daijiaping area. (**a**) Planar cross-bedding in the A11 well core data, at a depth of 2408.26 m; (**b**) Climbing-ripple cross-lamination in the A11 well core data, at a depth of 2398.3 m; (**c**) Parallel bedding in the A33 well core data, at a depth of 2412.8 m; (**d**) Lag deposits of muddy gravel at the bottom in the A11 well core data, at a depth of 2403.22 m; (**e**) Bottom scouring surface in the A11 well core data, at a depth of 2417.58 m; (**f**) Stratigraphic column and well log of a section of well A11.

4.1.3. Floodplain Microfacies

Description

Floodplain microfacies are divided into five typical FAs: parallel-bedded silty mudstone (Fm), horizontal-bedded argillaceous siltstone (Fm), ripple cross-laminated argillaceous siltstone (Sr), horizontal-bedded mudstone (Fm), and bioturbated argillaceous siltstone (Flb) (Figures 2 and 3, Table 1). Parallel-bedded silty mudstone facies, about 3 m thick, mainly consist of gray-white silty mudstone and develop parallel bedding. Horizontal-bedded argillaceous siltstone facies are mostly found in the lower part of the floodplain, about 1–3 m thick, primarily composed of gray-white argillaceous siltstone, and develop horizontal bedding. The top and bottom surfaces are surrounded by mudstone. Ripple cross-laminated argillaceous siltstone facies, about 2 m thick, are mainly composed of light gray argillaceous siltstone and develop ripple cross-lamination with numerous black carbon laminations (Figure 2b). Horizontal-bedded mudstone facies are mostly light gray or gray-black with reduced colors, containing a large amount of plant charcoal (Figure 3e) and exhibiting clear charcoal outlines. Bioturbated argillaceous siltstone facies are about 1 m thick, where high-angle inclined or nearly vertical dwelling burrows, about 5 cm long, can be observed in the gray-white argillaceous siltstone (Figure 3d). The gamma curve is a jagged line of high amplitude, with gamma values greater than 100 API (Figure 3f).

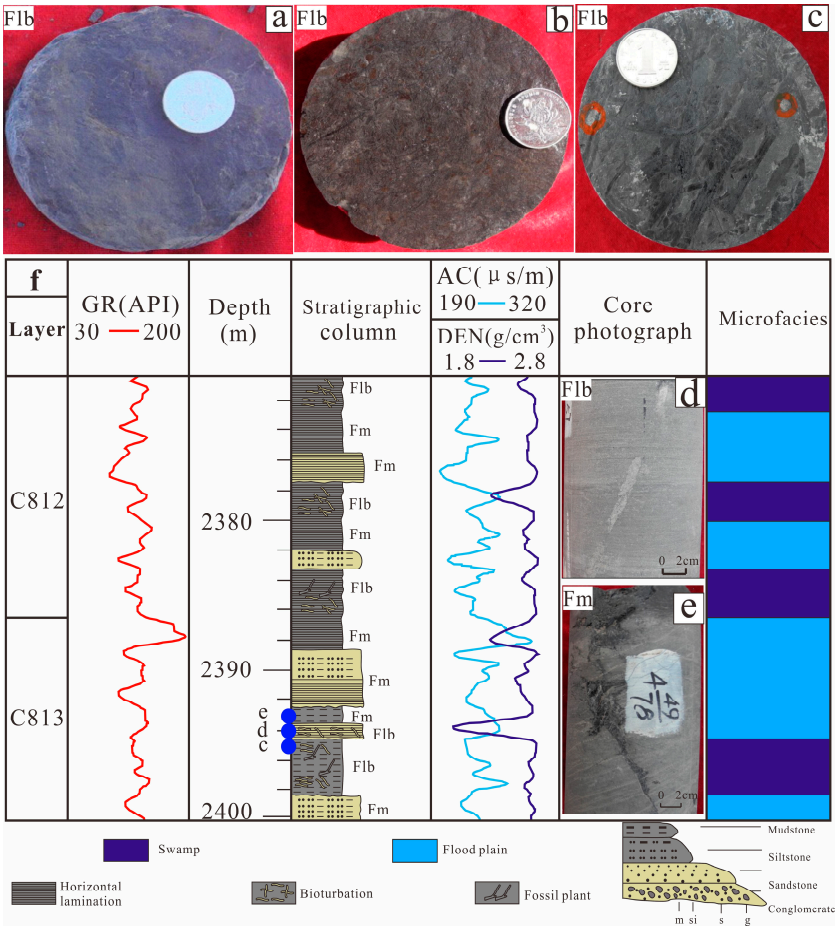

Figure 3. Photographs and stratigraphy of the Chang 8 member in Daijiaping area. (**a**) Gray black mudstone in the A34 well core data at a depth of 2027.51 m. (**b**) Plant root in the A35 well core data, at a depth of 2271.38 m; (**c**) Plant charcoal and burrow in the A33 well core data, at a depth of 2495.68 m; The red circles are biological burrows; (**d**) Burrow in the A33 well core data, at a depth of 2494.58 m; (**e**) Plant charcoal in the A33 well core data, at a depth of 2393.22 m; (**f**) Stratigraphic column and well log of a section of well A33.

Explanation

Ripple cross-lamination, plant charcoal, bioturbation, and obvious burrow traces in silty mudstone and argillaceous siltstone collectively reflect the floodplain depositional environment. Several siltstone-mudstone FAs indicate typical floodplain deposits formed by rivers under periodic flooding [42–44]. Fine-grained sediments deposited during floods formed finer mudstone, while coarse-grained sediments deposited during lateral movement of the riverbed formed coarser siltstone.

4.1.4. Swamp Microfacies

Description

Swamp microfacies are characterized by bioturbated mudstone facies (Flb) (Figure 2, Figure 3, Table 1). Bioturbated mudstone is dominated by gray-black mudstone (Figure 3a) and contains a large amount of plant charcoal (Figure 3c), exhibiting horizontal bedding and a bioturbated structure. Dwelling burrows have a diameter of about 0.5 cm (Figure 3c). Plant roots, oxidized to brown and appearing as irregular stripes, can be observed in shale (Figure 3b). The gamma curve is straight and jagged, with gamma values greater than 100 API (Figure 3f).

Explanation

The presence of black mudstone, plant charcoal, and plant roots in swamp microfacies indicates a warm and humid environment with sustained water availability. In such a stable and calm environment with adequate oxygen supply, biological activity thrives and vegetation grows. When the plants die, their remains are reduced to black organic matter and form peat deposits. The bioturbation and horizontal bedding observed in gray-black mudstones indicate a quiet, reducing, and calm depositional environment in the swampy lowland [45–47].

Table 1. Summary of Lithofacies Types Observed in C81 Member (Modified according to Zhu et al., 2020) [47].

Facies Code	Lithology	Sedimentary Structures	Depositional Process	Interpretation
Gpt	pebbly sandstone	massive structure, lag deposit (Figure 2d)	Hydrodynamic environment of traction flow [48,49]	When the water flow erodes the concave bank and riverbed at the maximum velocity, the velocity decreases, and coarse particles carried by the water flow are first deposited on the scouring surface, thus forming the bottom lag deposits
St	Sand, fine to medium-grained sandstone	Trough cross-bedded	Unidirectional low-flow environment [48]	The water flow further deviates to the convex bank. The water depth becomes shallow, and the flow velocity decreases, resulting in the deposition of fine and medium components in jumping components in turn and the formation of the dune bottom of dune facies. With the movement of sand dunes, trough cross-bedding formed [50]
Sr	argillaceous siltstone	Ripple cross-laminations (Figure 2b)	The lower part of the lower flow regime [51–53]	Asymmetrical current ripples, climbing-current ripples [47]
Sh	Sandstone to siltstone	Planar or subplanar lamination (Figure 2c)	Unidirectional high-flow environment [50,53,54]	The water flow starts deviating to the convex bank. The water depth becomes shallow, and the flow velocity decreases but is still fast, resulting in the deposition of coarse components in jumping components in turn and the formation of the flat bottom before parallel bedding [51]

Table 1. *Cont.*

Facies Code	Lithology	Sedimentary Structures	Depositional Process	Interpretation
Sp	Sand, fine to medium-grained sandstone	Planar cross-bedded (Figure 2a,e)	Unidirectional high flow mode, sand wave transformation [50,55]	The product of multiple migrations and swings of channel sand bodies, as well as vertical aggradation, may result from the lateral aggradation of the river island [56]
Flb	dark gray mudstone to siltstone, bioturbated	Massive or horizontal lamination, bioturbated (Figure 3a–d)	Sediment precipitates from suspension or solution [43,57]	A swampy or floodplain environment with a permanent body of water
Fm	Siltstone/ mudstone	Massive or laminated (Figure 3e)	Deposition from suspension [50]	Floodplain deposit under stable hydrodynamic conditions

4.2. Reservoir Characteristics of Thin-Bedded Tight Sandstone

The statistical results of sand body thickness for 42 wells in the study area reveal that all 42 wells in the C81 member of Daijiaping encountered sand bodies during drilling. C811 is mainly composed of mudstone. C812 exhibits the most developed sand body, with a thickness of 5–25 m. C813 has a relatively low development degree of sand bodies, with some wells having sand bodies larger than 15 m. Overall, the C81 member has relatively developed sand bodies. The sand body thickness of most wells is less than 15 m, indicating a typical thin sand body (Figure 4a).

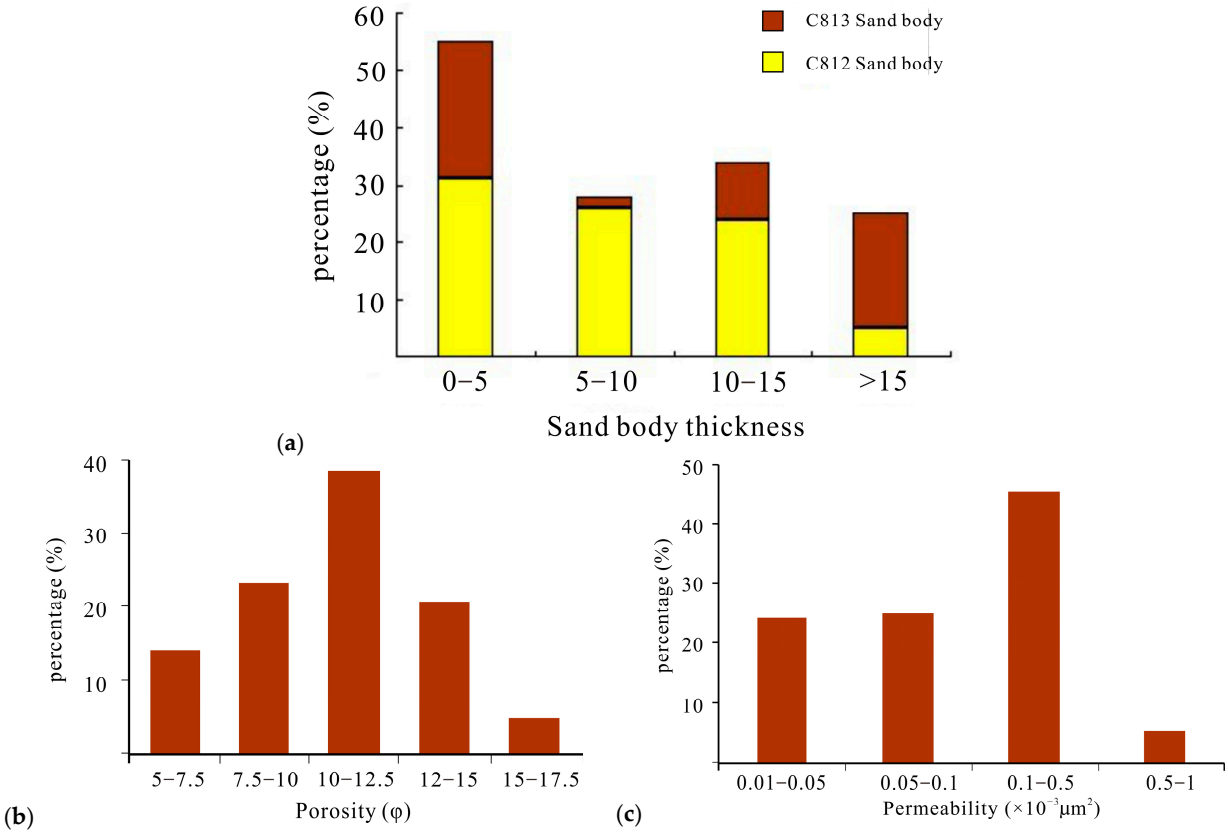

Figure 4. Lithology and physical property of core well in Daijiaping area. (**a**) Thickness distribution of reservoir sand body in C81 member. (**b**) Histogram of porosity distribution of C81 member reservoir. (**c**) Histogram of permeability distribution of C81 member reservoir.

Based on the statistical analysis for 238 core samples from 7 cored wells in the study area, the reservoir porosity of C81 members in Daijiaping is mainly distributed between 7.5% and 15%, with an average value of 11.7% (Figure 4b). The permeability mainly falls

within a range of 0.01–0.5 × 10^{-3} μm^2, with an average value of 0.2 × 10^{-3} μm^2 (Figure 4c), showing a typical tight reservoir.

4.3. Recognition and Distribution of Thin-Bedded Tight Sandstone

4.3.1. Stacking Pattern of Braided Channel Sand Body

After a detailed characterization of braided river sandstones, braided river tight sandstones were classified according to the stacking patterns of tight sandstones and their different distribution scales, including longitudinal incision, longitudinal separation, lateral shifting, and single channel types.

(1) Composite channel of longitudinal incision type

On a gentle and expansive floodplain, multiple river channels have undergone lateral migration and vertical stacking, influenced by the cyclical changes in floodwaters and erosion due to the river breaching and incision. As the channels undergo multiple cycles of migration, abandonment, and migration again, sedimentary units continue to accumulate laterally, resulting in a continuous vertical deposition. This process leads to the formation of complex sand body contacts over multiple periods [58].

Composite channel of longitudinal incision type refers to multi-stage channel multi-stage channel under vertical incision and stacking. Late-stage river channel deposits exhibit obvious erosion and scouring against early channel deposits during their formation. In this case, the two-stage sand bodies are vertically connected, with better connectivity, exhibiting a stacking pattern of the river channel to the river channel. The natural gamma curve in electrofacies shows a continuous box shape, while the seismic facies exhibit typical flat-top and convex-bottom lenticular seismic facies (Figure 5a).

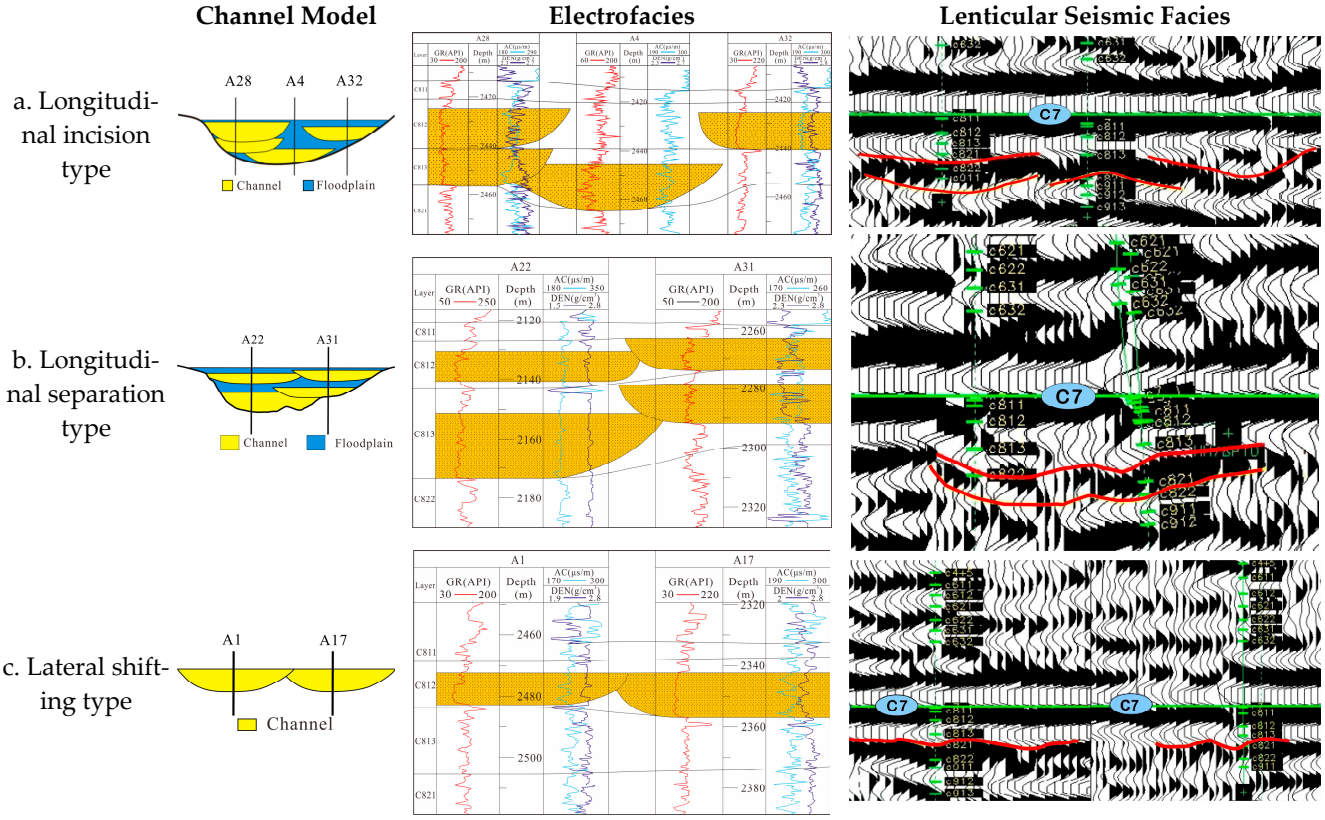

Figure 5. *Cont.*

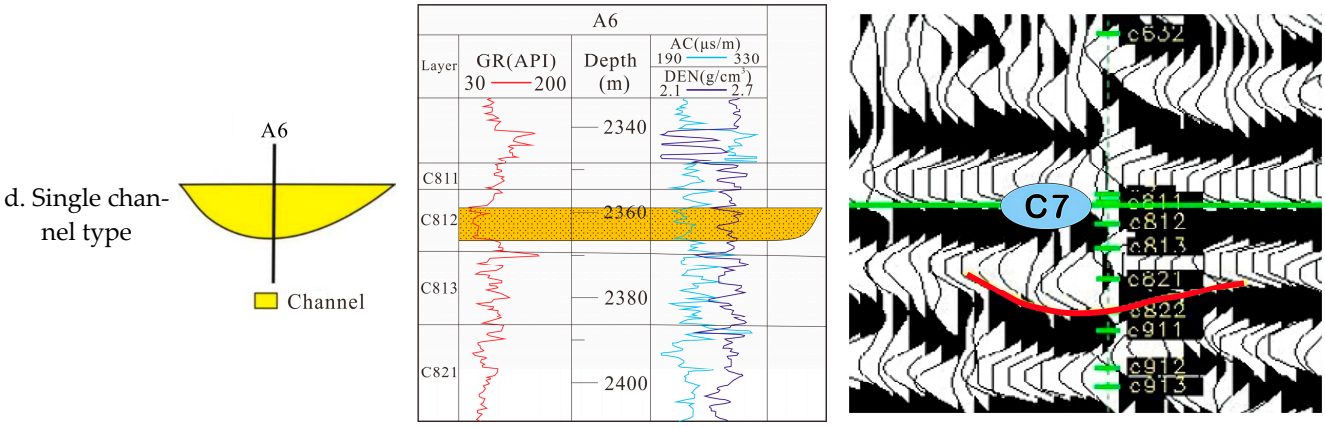

Figure 5. Seismic Response Characteristics of Braided Channel Reservoir Stacking Pattern. The solid blue lines in the lenticular seismic facies represent the Chang 7 member. The solid red lines in the lenticular seismic facies represent the bottom of the lenticular seismic facies. The green dotted lines in the lenticular seismic facies represent the well path.

(2) Composite channel of longitudinal separation type

Composite channel of longitudinal separation type refers to two-stage stacked sand bodies containing a mudstone interlayer. In other words, a suite of muddy floodplain sediments covers early river sediments, and late river sand bodies erode and are stacked on the floodplain, resulting in a stacking pattern of "channel-floodplain-channel". The longitudinal connectivity of sand bodies is poor. The natural gamma curve in electrofacies shows a shape of "box-shaped to jagged with a high amplitude, then to box-shaped" or "bell-shaped to jagged with a high amplitude, then to box-shaped". The seismic facies exhibit typical flat-top and convex-bottom lenticular seismic facies (Figure 5b).

(3) Composite channel of lateral shifting type

A composite channel of lateral shifting type is also called a confluence channel. As the accommodating space gradually decreases, rivers undergo channel migration, diversion, and multiple parallel channels, as well as a lateral accumulation over a short period. Sand bodies also migrate laterally, resulting in improved lateral connectivity. The natural gamma curve in electrofacies shows a box-shaped feature of a thin bed. The seismic facies exhibit flat-top and convex-bottom lenticular seismic facies with low amplitude (Figure 5c).

(4) Single channel

A single channel refers to a single isolated channel. The natural gamma curve in electrofacies shows a box-shaped feature of a thin bed. The seismic facies exhibit flat-top and convex-bottom lenticular seismic facies with low amplitude (Figure 5d).

4.3.2. Distribution Law of Braided River Tight Sandstone

The lateral extent of braided river sandstones observed after drilling can be presented using lenticular seismic facies observed after drilling as well-seismic data for sandstone calibration. Based on calibrated lenticular seismic facies of known well points, the extent of lenticular seismic facies for areas where no drilling is carried out is determined every 10 seismic lines, and then inter-well braided river sandstones are predicted (Figure 6a,c). The geometry of lenticular seismic facies also represents the extent of braided channel sand bodies, so the extent of braided channels can be characterized (Figure 6b,d) according to the extent of such lenticular seismic facies.

(1) Distribution characteristics of C812 sand body

C812 sand bodies had a banding distribution, and the channels were complex and varied, showing the typical characteristics of the braided channels, which also reflected the gradually dropping lake level during the depositional period and the decreasing accommodation, with sufficient sediment supply. The channel sand bodies have a thickness ranging from 4.5 to 23.9 m, and the channel width ranges from 300 to 1200 m. During the

C812 depositional period, the braided channels were mainly extended in the near north-east direction, and there were parts of small branches in the north-south direction, showing the north-east source direction in this period (Figure 6b).

(2) Distribution characteristics of C813 sand body

C813 sand bodies had a relatively simple distribution, and the channel branches were also significantly reduced, which indicated that the water and source supply upstream of the braided channel decreased during the C813 depositional period, resulting in the weakening of river diversion and the reduction of river branches. Additionally, more floodplain and swamp facies deposits were formed. The channel sand bodies have a thickness ranging from 3.1 to 25 m, and the channel width ranges from 400 to 1000 m. The channels were distributed in the near northeast direction, reflecting the northeast source direction during the C813 depositional period. A large number of floodplains and swamps were developed between the channels. (Figure 6d).

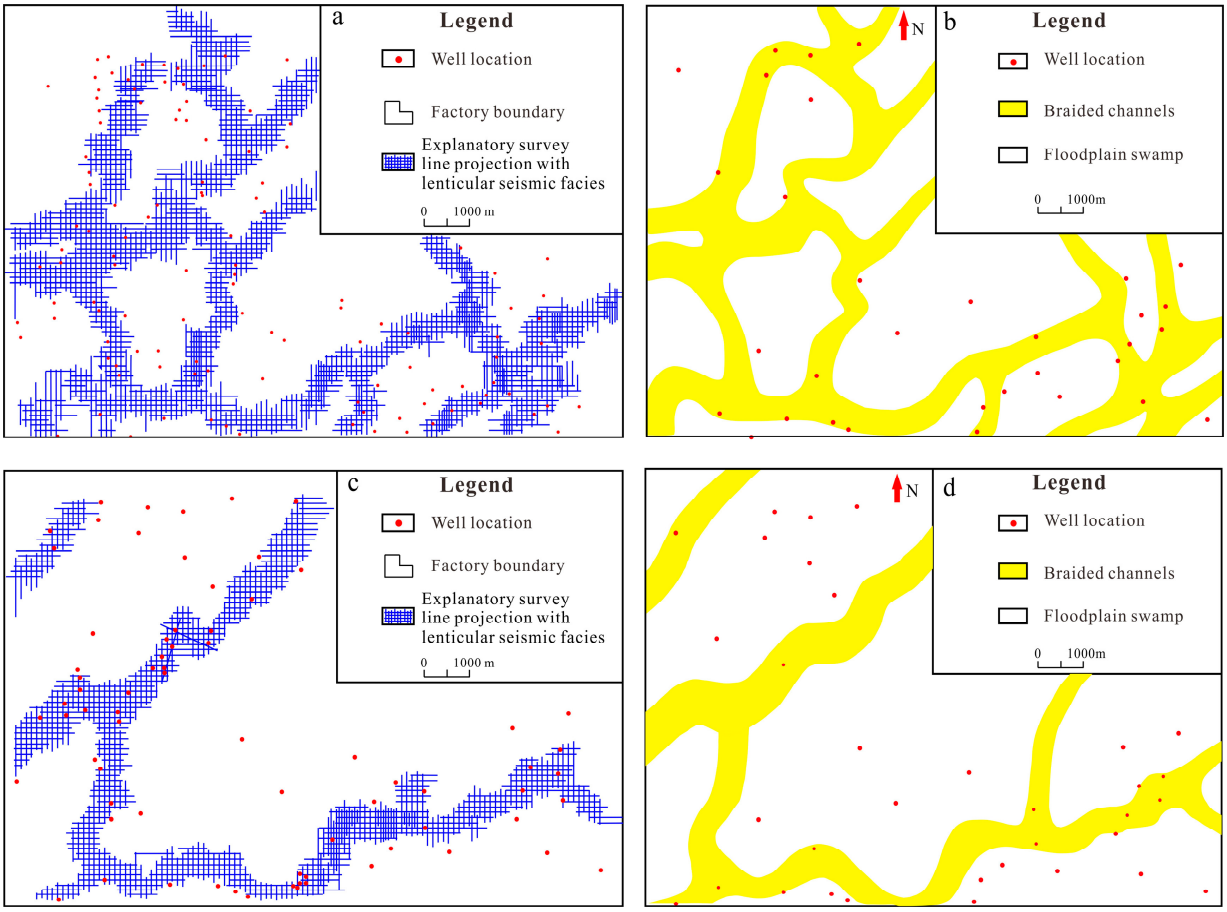

Figure 6. Distribution Plan of C8 Channel Sand Body (**a**) Distribution Map of Seismic Facies of C812 Channel Sand Body; (**b**) Distribution Plan of C812 Channel Sand Body; (**c**) Distribution Map of Seismic Facies of C813 Channel Sand Body; (**d**) Distribution Plan of C813 Channel Sand Body.

5. Discussion

5.1. Seismic Identification Method of Braided River Tight Sandstone

The Quaternary deep-bedded loess deposits in the Ordos Basin, ranging from tens to hundreds of meters thick, have accumulated over a long period of weathering and erosion. This has resulted in the formation of a unique loess landscape characterized by dendritic drainage patterns, gullies, tablelands, ridges, hills, slopes, and other landforms. The presence of loess layers with varying thicknesses, shallow underlying depths, and significant differences in intralayer velocity greatly impacts the absorption and attenuation of seismic wave energy, as well as the quality of seismic data recording [24,25]. A deep-bedded shale,

10–20 m thick, is deposited at the bottom of the C7 Member of the Yanchang Formation, forming a distinctive strong reflection lineup on seismic profiles. This suppresses the seismic reflection energy of the underlying thin-bedded sand body at the Chang 81 Member to some extent. Braided river sand bodies in the Chang 81 Member exhibit characteristics such as thin thickness, rapidly changing facies, and high heterogeneity. Furthermore, the wave impedance contrast between thin-bedded sand bodies and adjacent mudstones is not prominent. These factors make it challenging to predict thin-bedded sand bodies in the study area. Seismic attributes, freeze-drying microtomy of stratigraphic facies, and sparse impulse inversion constrained by well logging have all been tried but with poor results. As a result, this study integrates data such as core samples, drilling, and seismic information. A method of constrained correlation between seismic waveform and seismic facies was used to identify braided river thin-bedded sandstones in the Chang 81 Member, Daijiaping, Ordos Basin.

5.2. Quantitative Prediction of Braided Channel Scale

Through modern river deposit surveys and detailed analysis of ancient outcrops, scholars both at home and abroad have conducted quantitative prediction and identification of different types of river channel sand bodies and found that there is a quantitative constraint relationship between the bankfull width of a river and its maximum depth [59–65]. However, it is difficult to determine whether the thickest part of the sand body is encountered during drilling solely by observing the sandstone thickness during drilling (i.e., whether it is at the maximum depth of the river). This makes predicting the width of river channels using the observed sandstone thickness during drilling associated with significant error.

In this study, lenticular seismic facies were identified to predict braided river sandstones, with the shale marker bed at the bottom of the C7 member corrected to a flat reference surface. The geometry of lenticular seismic facies represents the overall geometry of braided river sand bodies. Therefore, the distance (W) between two points (Figure 7, points a, b) when the waveform starts to bend down continuous wave peak lineups (or white wave trough lineups) at black-filled variable areas on waveform profiles of lenticular seismic facies represents the braided river bankfull width. The maximum depth of the river is represented by the distance (H) between the tangent point (Figure 7, point c) of the lower curve of wave peak lineups (or white wave trough lineups) and the horizontal plane and points a, b. This method is sufficient to count the bankfull width and maximum depth of the river using calibrated braided river seismic facies observed during drilling for all sand bodies.

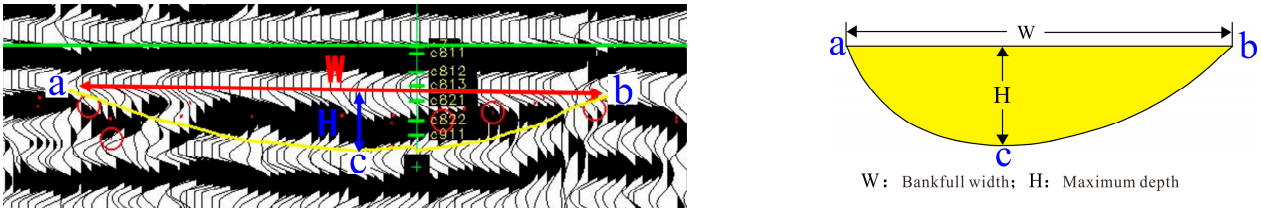

(**a**) (**b**)

Figure 7. Relationship between River Parameters W and H under Lenticular Seismic Facies of Braided Channels. (**a**) Relation between W and H of channel in seismic profile; (**b**) Schematic diagram of W and H model of channel lens.

According to the bankfull width (W) and the maximum depth (H, time domain) based on braided river lenticular seismic facies for 32 wells in the study area, the width of braided rivers in the study area falls within a range of 1140–6170 m, and the maximum thickness of braided river channel sand bodies is between 8.2–32.3 ms (Table 2). By fitting 32 sets of bankfull width and maximum depth from 32 wells in the study area, a quantitative

prediction formula for the width-to-thickness ratio of braided channel scale is obtained as follows (Figure 8):

$$y = 228.36x - 1447 \qquad R^2 = 0.8768 \qquad (1)$$

where: x = Maximum depth (ms);

y = Bankfull width (m);

If the maximum depth (ms) of the channel lens is read on seismic profiles, the bankfull width of the channel lens can be calculated by the formula (1) to realize the quantitative forecasting of the size of the channel lens, thus providing accurate guidance for well location deployment.

Table 2. Statistical Table of Channel Sand Body Parameters under Lenticular Seismic Facies of Braided Channels in Chang 81 Member.

Well Name	Maximum Depth (ms)	Bankfull Width (m)	Well Name	Maximum Depth (ms)	Bankfull Width (m)
A1	8.2	1140	A17	22	2600
A2	14.3	1350	A18	19	2721
A3	16	1500	A19	23.2	3160
A4	12.8	1523	A20	20	3376
A5	16	1530	A21	17.5	3490
A6	12	1680	A22	23	3780
A7	18	1820	A23	22.2	4050
A8	16.7	1860	A24	24	4441
A9	15	1950	A25	25	4441
A10	14.7	1960	A26	23.7	4722
A11	16.5	2030	A27	32.3	5180
A12	15.3	2081	A28	27.5	5250
A13	16.5	2140	A29	32	5380
A14	15.3	2160	A30	30	5420
A15	16.2	2280	A31	27.5	5971
A16	15	2420	A32	31.4	6170

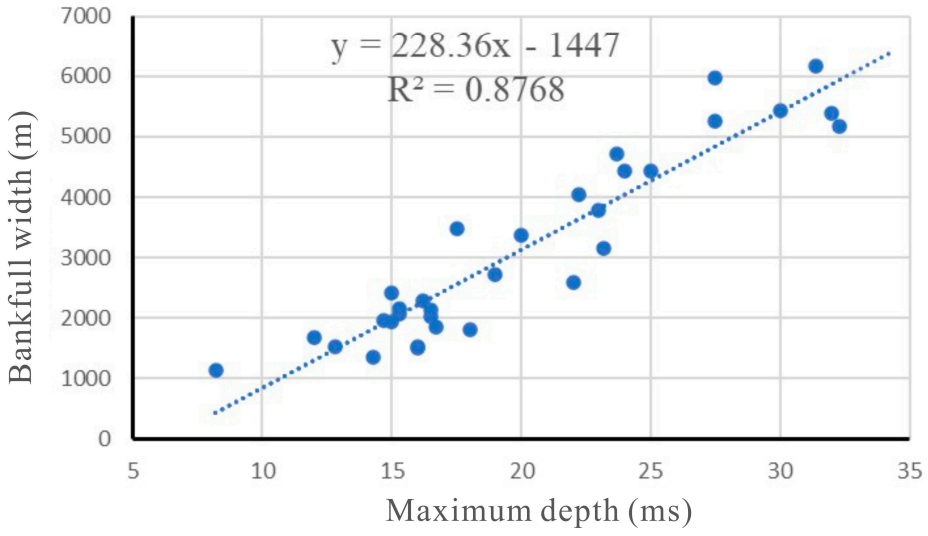

Figure 8. Chang 81 Member Fitting Formula for Bankfull Width and Maximum Depth in Chang 81 Member.

5.3. Influence of Seismic Facies Distribution on Horizontal Well Deployment

The lenticular seismic facies of well seismic calibration have two advantages: (1) the relative position relationship between well location and channel sand body can be intuitively and accurately determined in the profile (Figure 9); (2) it can guide the drilling direction of horizontal wells more accurately. The horizontal section of well A31 was deployed by drilling from the middle of the channel towards the side of the channel (Figure 9a), with an average daily oil production of 0.41t (Figure 10a). On the contrary, for well A36, the horizontal section was drilled from the side of the channel towards the middle of the channel (Figure 9b), with an average daily oil production of 0.72 t (Figure 10b). By comparison, if horizontal wells are deployed from the side of the sand body towards the center of the sand body in a river channel, the corresponding production is 1.8 times higher than that of horizontal wells deployed oppositely, leading to an average daily production increase of 75%. This shows that thin-bedded tight sandstones in braided channels, characterized by top-flat and bottom-convex lenticular seismic facies, have practical significance in guiding the deployment of horizontal well patterns for tight oil and improving oil and gas recovery.

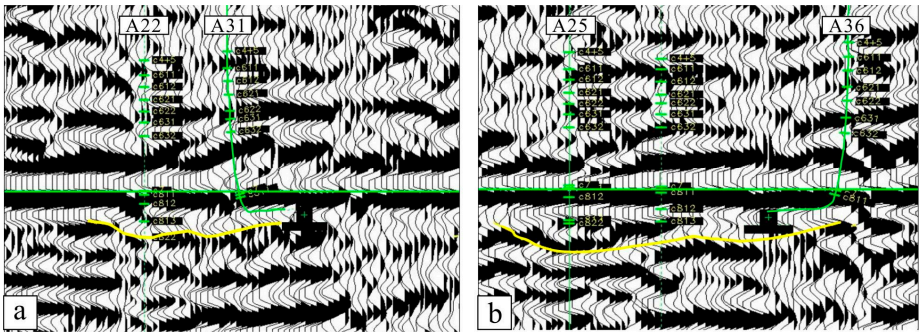

Figure 9. Two Different Horizontal Well Drilling Schemes under the Guidance of Seismic Facies. (**a**) A31 Well Drilled from the Middle of the Channel towards the Side of the Channel; (**b**) A36 Well Drilled from the Side of the Channel towards the Middle of the Channel.

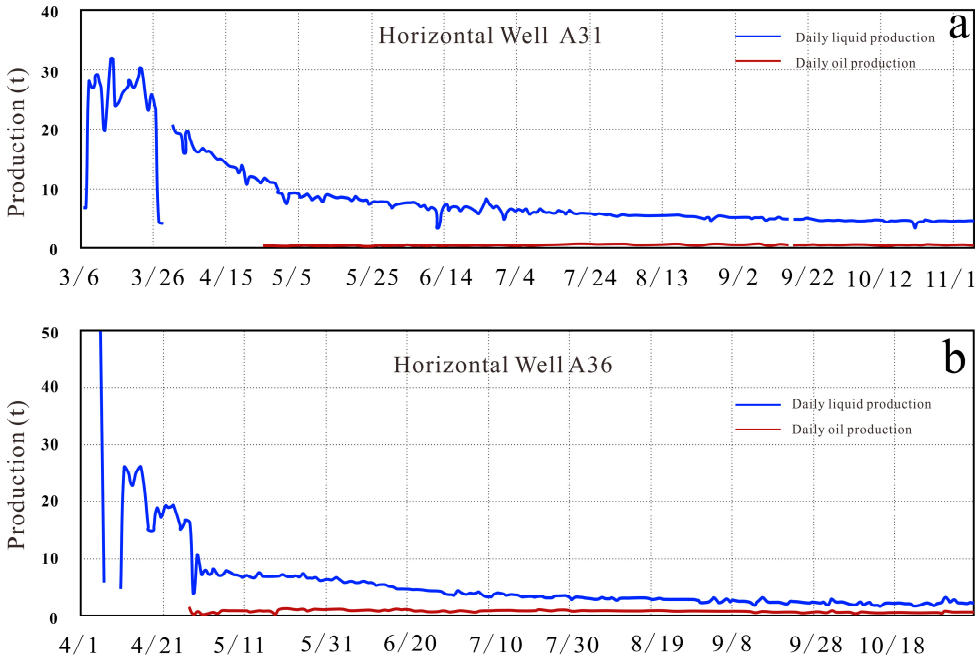

Figure 10. Comparison of Production under Two Different Horizontal Well Drilling Schemes. (**a**) Production of Horizontal Well A31; (**b**) Production of Horizontal Well A36.

6. Conclusions

This study integrates data from core samples, drilling, and seismic information to identify braided river thin-bedded sandstones in the Chang 81 Member at Daijiaping, Ordos Basin, using a method of constrained correlation between seismic waveform and seismic facies. This approach aids in determining the sedimentary microfacies types and reservoir characteristics of thin-bedded tight sandstones. We establish a quantitative fitting formula for the width-to-thickness ratio of braided channel sand bodies to finely characterize sand body stacking patterns and spatial distribution of thin-bedded tight sandstones in braided channels. The following conclusions were achieved from this study:

(1) Braided delta plain deposits developed in the Chang 81 Member in Daijiaping primarily consist of four types of sedimentary microfacies: braided channel, crevasse channel, floodplain, and swamp. The sand body thickness of Chang 81 Member is mainly concentrated between 5–25 m. It has low porosity and permeability, making it a typical thin-bedded tight sandstone reservoir.

(2) A method of constrained correlation between seismic waveform and seismic facies was used to identify braided river thin-bedded sandstones in the Chang 81 Member and to summarize four sand body stacking patterns, including the longitudinal incision type, longitudinal separation type, lateral shifting type, and single channel type. In addition, a quantitative forecasting formula of the width-to-thickness ratio was established for the river channel scale to provide accurate guidance for well deployment.

(3) If horizontal wells are deployed from the side of the sand body towards the center of the sand body in a river channel, the corresponding production is 1.8 times higher than that of horizontal wells deployed in the opposite direction.

Therefore, thin-bedded tight sandstones in braided channels, characterized by top-flat and bottom-convex lenticular seismic facies, have practical significance in guiding the deployment of horizontal well patterns for tight oil and improving oil and gas recovery.

Author Contributions: Conceptualization, T.L. and C.F.; methodology, T.L. and C.F.; software, M.S. and Z.C.; validation, T.L. and C.F.; formal analysis, M.S.; investigation, T.L.; resources, C.F.; data curation, T.L.; writing—original draft preparation, T.L.; writing—review and editing, T.L. and C.F.; visualization, M.S.; supervision, M.S.; project administration, C.F.; funding acquisition, C.F. All authors have read and agreed to the published version of the manuscript.

Funding: This research was supported by the National Natural Science Foundation of China (Grant no. 41502127), the Natural Science Basic Research Plan in Shaanxi Province of China (Grant nos. 2017JM4013; 2020JQ798), and the Scientific Team Foundation of the Department of Geology, Northwest University, Xian.

Data Availability Statement: Not applicable.

Conflicts of Interest: The authors declare no conflict of interest. All authors have confirmed.

References

1. Osinowo, O.O.; Ayorinde, J.O.; Nwankwo, C.P.; Ekeng, O.M.; Taiwo, O.B. Reservoir description and characterization of Eni field Offshore Niger Delta, southern Nigeria. *J. Pet. Explor. Prod. Technol.* **2018**, *8*, 381–397. [CrossRef]
2. Adelu, A.O.; Aderemi, A.A.; Akanji, A.O.; Sanuade, O.A.; Kaka, S.I.; Afolabi, O.; Olugbemiga, S.; Oke, R. Application of 3d static modeling for optimal reservoir characterization. *J. Afr. Earth Sci.* **2019**, *152*, 184–196. [CrossRef]
3. Zhang, G.; Feng, C.; Yao, X. Petroleum Geology in Deepwater Settings in a Passive Continental Margin of a Marginal Sea: A Case Study from the South China Sea. *Acta Geol. Sin. Engl. Ed.* **2021**, *95*, 1–20. [CrossRef]
4. Qadri, S.; Ahmed, W.; Haque, A.; Radwan, A.E.; Hakimi, M.H.; Aal, A. Murree clay problems and water-based drilling mud optimization: A case study from the Kohat basin in northwestern Pakistan. *Energies* **2022**, *15*, 3424. [CrossRef]
5. Haque, A.E.; Qadri, S.; Bhuiyan, M.; Navid, M.; Nabawy, B.S.; Hakimi, M.H.; Abd-El-Aal, A.K. Integrated wireline log and seismic attribute analysis for the reservoir evaluation: A case study of the Mount Messenger Formation in Kaimiro Field, Taranaki Basin, New Zealand. *J. Nat. Gas Sci. Eng.* **2022**, *99*, 104452. [CrossRef]
6. Castagna, J.P.; Sun, S.; Siegfried, R.W. Instantaneous spectral analysis: Detection of low-frequency shadows associated with hydrocarbons. *Lead. Edge* **2003**, *22*, 120–127. [CrossRef]
7. Holditch, S.A. Tight gas sands. *J. Pet. Technol.* **2006**, *58*, 86–93. [CrossRef]

8. Goloshubin, G.; Schuyver, C.V.; Korneev, V.; Silin, D.; Vingalov, V. Reservoir imaging using low frequencies of seismic reflections. *Lead. Edge* **2012**, *25*, 513–672. [CrossRef]
9. Quintal, B.; Schmalholz, S.M.; Podladchikov, Y.Y. Low-frequency reflections from a thin layer with high attenuation caused by interlayer flow. *Geophysics* **2009**, *74*, Y7. [CrossRef]
10. Zhou, Z.; Zhang, H.; Cao, G.; Ma, Y.; He, S.; Zhou, T. Application of maximum entropy spectrum decomposition in quantitative prediction of thin sand body in meandering river. *Fault Block Oil Gas Field* **2019**, *26*, 719–722.
11. Colombera, L.; Mountney, N.P.; Medici, G.L.; West, L.J. The geometry of fluvial channel bodies: Empirical characterization and implications for object-based models of the subsurface. *AAPG Bull.* **2019**, *103*, 905–929. [CrossRef]
12. Chen, S.; Wu, Y.; Fu, X.; Zhang, W.; An, Z.; Cong, P. Fine Portray of Thin Sand-Bodies and Trajectory Design of Horizontal Well in Zhaoyuan Area. *J. Jilin Univ. Earth Sci. Ed.* **2020**, *50*, 598–607.
13. Cao, S.; Sun, Z.; Dang, H.; Cao, S.; Liu, D.; Hu, S. Prediction technology of tight oil thin sand reservoir and its application effect: A case study of Lower Cretaceous Quantou Formation in Aonan block, Songliao Basin. *Lithol. Reserv.* **2021**, *33*, 239–247.
14. Liu, L.; Guan, M.; Zhang, X.; Zhu, Y.; Lv, H.; Meng, C. Frequency information extraction based on time-frequency ridges for characterizing thin sand bodies. *J. Geophys. Eng.* **2022**, *19*, 167–177. [CrossRef]
15. Jiang, Z.; Lin, S.; Pang, X. The comparison of two types of tight sand gas reservoir. *Pet. Geol. Exp.* **2006**, *28*, 210–218. (In Chinese with English Abstract)
16. Dong, X.; Mei, L.; Quan, Y. Types of tight sand gas accumulation and its exploration prospect. *Nat. Gas Geosci.* **2007**, *18*, 351–355. (In Chinese with English Abstract)
17. Ringrose, P.S.; Sorbie, K.S.; Corbett, P.W.M.; Jensen, J.L. Immiscible flow behaviour in laminated and cross-bedded sandstones. *J. Pet. Sci. Eng.* **1993**, *9*, 103–124. [CrossRef]
18. Medici, G.; West, L.J. Review of groundwater flow and contaminant transport modelling approaches for the Sherwood Sandstone aquifer, UK; insights from analogous successions worldwide. *Q. J. Eng. Geol. Hydrogeol.* **2022**, *55*, qjegh2021-176. [CrossRef]
19. Yu, X.; Li, S.; Yang, Z. Discussion on deposition-diagenesis genetic mechanism and hot issues of tight sandstone gas reservoir. *Lithol. Reserv.* **2015**, *27*, 1–13.
20. Tong, X.; Guo, B.; Li, J. Comparison study on accumulation & distribution of tight sandstone gas between China and the United States and its significance. *Eng. Sci.* **2012**, *14*, 9–15.
21. Zhang, S.; Ding, X.; Wan, Y. Formation mechanism and distribution of clay minerals of deeply tight siliciclastic reservoirs. *J. Southwest Pet. Univ. Sci. Technol. Ed.* **2012**, *34*, 174–182.
22. Zheng, J.; Ying, F. Reservoir characteristics and diagenetic model of sandstone intercalated in coal-bearing strata (acid water medium). *Acta Pet. Sin.* **1997**, *18*, 19–24.
23. Wang, D.; Zhang, M.; Yang, W.; Cai, K.; Gao, L.; Zhu, J. Seismic forward and inverse simulation in a tight reservoir model of loess plateau region. *Pet. Explor. Dev.* **2017**, *44*, 265–273. [CrossRef]
24. Wang, W.; Wang, X.; Zeng, H.; Liang, Q. Preconditioning point-source/point-receiver high-density 3D seismic data for lacustrine shale characterization in a loess mountain area. *Interpretation* **2017**, *5*, 1M-T277. [CrossRef]
25. Chen, S.; Fan, S.; Wang, X. Neotectonic movement in the southern margin of the Ordos Block inferred from the Qianhe River terraces near the north of the Qinghai–Tibet Plateau. *Geol. J.* **2018**, *53*, 274–281. [CrossRef]
26. Liu, C.; Zhao, H.; Sun, Y. Tectonic background of ordos basin and its controlling role for basin evolution and energy mineral deposits. *Energy Explor. Exploit.* **2009**, *27*, 15–27. [CrossRef]
27. Li, J.; Li, J.; Li, Z.S.; Zhang, C.; Cui, H.; Zhu, Z. Characteristics and genetic types of the Lower Paleozoic natural gas, Ordos Basin. *Mar. Pet. Geol.* **2018**, *89*, 106–119. [CrossRef]
28. Fu, J.; Dong, G.; Zhou, X.; Hui, X.; Dan, W.; Fan, L.; Wang, Y.; Zhang, H.; Gu, Y.; Zhou, G. Research progress of petroleum geology and exploration technology in Ordos Basin. *China Pet. Explor.* **2021**, *26*, 19–40.
29. Zhang, W.; Yang, H.; Li, S. Hydrocarbon accumulation significance of Chang 9^1 high-quality lacustrine source rocks of Yanchang Formation, Ordos Basin. *Pet. Explor. Dev.* **2008**, *35*, 557–562. [CrossRef]
30. Zhao, Y.; Yao, J.; Duan, Y.; Wu, Y.; Cao, X.; Xu, L.; Chen, S. Oil-source Analysis for Chang-9 Subsection (Upper Triassic) of Eastern Gansu Province in Ordos Basin. *Acta Sedimentol. Sin.* **2015**, *33*, 1023–1032.
31. Wang, B.; Sun, W.; Bai, Y.; Han, J.; Liu, D.; Zhang, X. Diagenesis and Pore Evolution of Tight Sandstone Reservoir of Chang 6-1 Member in Jiyuan Area, Ordos Basin. *Xinjiang Pet. Geol.* **2018**, *39*, 430–438.
32. Zhou, X.; He, S.; Chen, Z.Y.; Wang, F.; Zhou, S.; Liu, P. Diagenesis and diagenetic facies of low porosity and permeability sandstone in Member 8 of the Yanchang Formation in Daijiaping area, Ordos Basin. *Oil Gas Geol.* **2016**, *37*, 155–164.
33. Li, D. Return to petroleum geology of Ordos Basin. *Pet. Explor. Dev.* **2004**, *31*, 207–215.
34. Wang, X.; Guo, P.; Fu, J.; Liu, H.; Chen, Q.; Li, T.; Liao, J.; Zhang, C. Control factors for forming higher porosity and permeability sandstone reservoirs in the Chang 8 member of Yanchang Formation, Ordos Basin. *Pet. Explor. Dev.* **2005**, *32*, 35–38.
35. Zhu, X.; Deng, X.; Liu, Z.; Sun, B.; Liao, J.; Hui, X. Sedimentary characteristics and model of shallow braided delta in large-scale lacustrine: An example from Triassic Yanchang Formation in Ordos Basin. *Earth Sci. Front.* **2013**, *20*, 19–28.

36. Feng, C.; Yao, X.; Yang, H. Source-Sink System and Sedimentary Model of Progradational Fan Delta Controlled by Restricted Ancient Gully: An Example in the Enping Formation in the Southern Baiyun Sag, Pearl River Mouth Basin, Northern South China Sea. *Acta Geol. Sin. Engl. Ed.* **2021**, *95*, 232–247. [CrossRef]
37. Best, J.L.; Ashworth, P.J.; Bristow, C.S.; Roden, J. Three-dimensional sedimentary architecture of a large, mid-channel sand braid bar, Jamuna river, Bangladesh. *J. Sediment. Res.* **2003**, *73*, 516–530. [CrossRef]
38. Smith, G.; Ashworth, P.J.; Best, J.L.; Woodward, J.; Simpson, C.J. The sedimentology and alluvial architecture of the sandy braided South Saskatchewan River, Canada. *Sedimentology* **2010**, *53*, 413–434. [CrossRef]
39. Ashworth, P.J.; Smith, G.; Best, J.L.; Bridge, J.S.; Lane, S.N.; Lunt, I.A.; Reesink, A.J.H.; Simpson, C.J.; Thomas, R.E. Evolution and sedimentology of a channel fill in the sandy braided South Saskatchewan River and its comparison to the deposits of an adjacent compound bar. *Sedimentology* **2011**, *58*, 1860–1883. [CrossRef]
40. Parker, N.O.; Smith, G.H.S.; Ashworth, P.J.; Best, J.L.; Lane, S.N.; Lunt, I.A.; Simpson, C.J.; Thomas, R. Quantification of the relation between surface morphodynamics and subsurface sedimentological product in sandy braided rivers. *Sedimentology* **2012**, *60*, 820–839. [CrossRef]
41. Du, W.; Jiang, Z.; Zhang, Y.; Xu, J. Sequence stratigraphy and sedimentary facies in the lower member of the Permian Shanxi formation, northeastern Ordos Basin, China. *J. Earth Sci.* **2013**, *24*, 75–88. [CrossRef]
42. Bridge, J.S.; Jalfin, G.A.; Georgieff, S.M. Geometry, lithofacies, and spatial distribution of cretaceous fluvial sandstone bodies, san Jorge basin, Argentina: Outcrop analog for the hydrocarbon-bearing chubut group. *J. Sediment. Res.* **2000**, *70*, 341–359. [CrossRef]
43. Ghazi, S.; Mountney, N.P. Facies and architectural element analysis of a meandering fluvial succession: The Permian Warchha Sandstone, Salt Range, Pakistan. *Sediment. Geol.* **2009**, *221*, 99–126. [CrossRef]
44. Mrinjek, E.; Sremac, J.; Velic, J. Pliocene alluvial sediments in the Drava depression of the Virovitica-Slatina Area, northern Croatia. *Geol. Croat.* **2006**, *59*, 65–84. [CrossRef]
45. Fielding, C.R. Upper delta plain lacustrine and fluviolacustrine facies from the Westphalian of the Durham coalfield, NE England. *Sedimentology* **1984**, *31*, 547–567. [CrossRef]
46. Jin, Z.; Gu, J.; Su, N.; Huang, W. Depositional characteristics and petroleum geological significance of wetland. *Pet. Sci.* **2009**, *6*, 347–353. [CrossRef]
47. Zhu, Z.; Kuang, H.; Liu, Y.; Zhai, Q. Intensifying aeolian activity following the end-Permian mass extinction: Evidence from the Late Permian–Early Triassic terrestrial sedimentary record of the Ordos Basin, North China. *Sedimentology* **2020**, *67*, 2691–2720. [CrossRef]
48. Miall, A.D. A review of the braided-river depositional environment. *Earth-Sci. Rev.* **1997**, *13*, 1–62. [CrossRef]
49. Medici, G.; Boulesteix, K.; Mountney, N.P.; West, L.J.; Odling, N.E. Palaeoenvironment of braided fluvial systems in different tectonic realms of the triassic sherwood sandstone group, UK. *Sediment. Geol.* **2015**, *329*, 188–210. [CrossRef]
50. Ma, S.; Yang, Q. The depositional model, 3-D architecture and heterogeneous modle of point bar in meandering channels. *Acta Sedimentol. Sin.* **2000**, *18*, 241–247.
51. Miall, A.D. Lithofacies types and vertical profile models in braided river deposits: A summary. In *Fluvial Sedimentology*; Miall, A.D., Ed.; Canadian Society of Petroleum Geologists: Calgary, AB, Canada, 1978; Volume 5, pp. 597–604.
52. Postma, G. Depositional architecture and facies of river and fan deltas: A synthesis, coarse grained deltas. *Spec. Publ. Int. Assoc. Sediment.* **1990**, *10*, 13–28.
53. Horton, B.K.; Schmitt, J.G. Sedimentology of the lacustrine fan-delta system, Miocene Horse Camp Formation Nevada, USA. *Sedimentology* **1996**, *43*, 133–155. [CrossRef]
54. Clemmensen, L.B.; Øxnevad, I.E.I.; Boer, P. *Climatic Controls on Ancient Desert Sedimentation: Some Late Palaeozoic and Mesozoic Examples from NW Europe and the Western Interior of the USA*; Wiley-Blackwell: Hoboken, NJ, USA, 2014.
55. Miall, A.D. Reservoir heterogeneities in fluvial sandstones; lessons from outcrop studies. *Am. Assoc. Pet. Geol. Bull.* **1988**, *72*, 682–697.
56. Qi, R.; Li, L.; Qin, X. Sand body configuration and gas-bearing properties of near source sand-gravel braided river on the northern margin of Ordos Basin. *Pet. Geol. Exp.* **2019**, *41*, 682–690.
57. Mall, A.D. *The Geology of Fluvial Deposits*; Springer: Berlin/Heidelberg, Germany, 1996.
58. Zou, T. Study on superimposition patterns and main remaining oil control factors of channel sand-bodies. *J. Xi'an Shiyou Univ. Nat. Sci. Ed.* **2017**, *32*, 36–41.
59. Leopold, L.B.; Wolman, M.G. River channel patterns—Braided, meandering and straight. *Prof. Geogr.* **1957**, *9*, 39–85.
60. Schumm, S.A. Sinuosity of alluvial rivers on the Great Plains. *Bull. Geol. Soc. Am.* **1963**, *74*, 1089–1099. [CrossRef]
61. Leeder, M.R. Fluviatile fining-upwards cycles and the magnitude of palaeochannels. *Geol. Mag.* **1973**, *110*, 265–276. [CrossRef]
62. Lorenz, J.C.; Clark, J.A.; Heinze, D.M. Determination of widths of meander-belt sandstone reservoirs from vertical downhole data, Mesaverde group, Piceance Creek basin, Colorado. *AAPG Bull.* **1985**, *69*, 710–721.
63. Bridge, J.S. The interaction between channel geometry, water flow, sediment transport and deposition in braided rivers. *Geol. Soc. Lond. Spec. Publ.* **1993**, *75*, 13–71. [CrossRef]

64. Davies, D.K.; Williams, B.P.J.; Vessell, R.K. Reservoir geometry and internal permeability distribution in fluvial, tight, gas sandstones, Travis Peak formation, Texas. *SPE Reserv. Eng.* **1993**, *8*, 7–12. [CrossRef]
65. Tan, C.; Yu, X.; Li, S.; Shan, X.; Chen, B. Sedimentology and stratigraphic evolution of the fan delta at the Badaowan formation (lower Jurassic), Southern Junggar Basin, Northwest China. *Arab. J. Geosci.* **2016**, *9*, 115. [CrossRef]